

Signatures of dark excitons in exciton-polariton optics of transition metal dichalcogenides

Beatriz Ferreira,^{1,*} Roberto Rosati,² Jamie M. Fitzgerald,² and Ermin Malic^{2,1}

¹*Chalmers University of Technology, Department of Physics, 412 96 Gothenburg, Sweden*

²*Department of Physics, Philipps-Universität Marburg, Renthof 7, D-35032 Marburg, Germany*

Integrating 2D materials into high-quality optical microcavities opens the door to fascinating many-particle phenomena including the formation of exciton-polaritons. These are hybrid quasi-particles inheriting properties of both the constituent photons and excitons. In this work, we investigate the so-far overlooked impact of dark excitons on the momentum-resolved absorption spectra of hBN-encapsulated WSe₂ and MoSe₂ monolayers in the strong-coupling regime. In particular, thanks to the efficient phonon-mediated scattering of polaritons into energetically lower dark exciton states, the absorption of the lower polariton branch in WSe₂ is much higher than in MoSe₂. It shows unique step-like increases in the momentum-resolved profile indicating opening of specific scattering channels. We study how different externally accessible quantities, such as temperature or mirror reflectance, change the optical response of polaritons. Our study contributes to an improved microscopic understanding of exciton-polaritons and their interaction with phonons, potentially suggesting experiments that could determine the energy of dark exciton states via momentum-resolved polariton absorption.

I. INTRODUCTION

Monolayers of transition metal dichalcogenides (TMDs) show a rich exciton landscape, including bright and dark exciton states [1, 2]. This class of atomically-thin materials exhibits a large oscillator strength and exciton binding energies in the range of a few hundreds of meV, hence governing the optoelectronic properties even at room temperature [1, 3–6]. TMDs have already been successfully integrated into optical cavities [7–9], where the coupling of cavity photons with excitons gives rise to the formation of exciton-polaritons [10, 11]. It is only the bright exciton states that can couple to photons to form these quasi-particles, while momentum-dark excitons [1, 2, 12] cannot be directly accessed by light. Nonetheless, these states are available scattering partners for polaritons via the interaction with phonons. The presence of dark excitons is expected to significantly change the polariton-phonon scattering rates, especially for tungsten-based TMDs, since here dark excitons are the energetically lowest states [13–16]. So far, polariton-phonon interactions in TMDs have not been well studied, leaving many open questions on the impact of dark exciton states on polariton absorption.

In our previous work, we studied transport properties of exciton-polaritons in MoSe₂ monolayers [17],

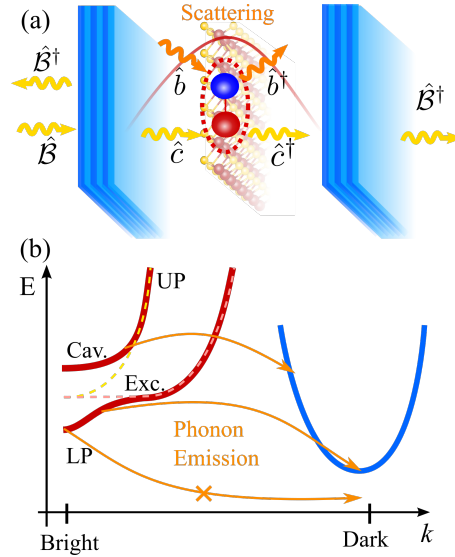


FIG. 1. (a) Schematic illustration of a TMD monolayer in a Fabry-Perot cavity with the fundamental cavity mode represented by the red curve. TMD excitons interact with photons and phonons as indicated by the creation (annihilation) operators for photons (\hat{c}^\dagger (\hat{c})) and phonons (\hat{b}^\dagger (\hat{b})). The cavity system interacts with the outside world via the operators \hat{B}^\dagger (\hat{B}). (b) Exciton-polariton band structure, where polaritons can scatter into dark exciton states by emitting phonons if momentum and energy can be conserved.

where dark excitons do not play an important role as they are energetically higher than the 1s bright states [1, 12, 14]. Now, the focus lies on the optical

* beatriz.ferreira@chalmers.se

response of polaritons in WSe₂ monolayers, specifically addressing the impact of dark exciton states. In this regard, the polariton absorption is especially informative as it unambiguously demonstrates strong coupling via the Rabi splitting [18], and its magnitude is determined by the balance between the polariton-phonon and cavity decay rates. We microscopically calculate the polariton absorption by combining the Heisenberg-Langevin equations [19] for polaritons with the exciton density matrix formalism [20, 21]. We calculate the full valley- and momentum-dependent polariton-phonon scattering rates that govern the optical response of TMD materials via both spectral linewidths and magnitude. In particular, we explore this in the context of the critical coupling condition [22], where the total cavity decay rate coincides with the polariton-phonon scattering rate. We predict that the presence of dark excitons has a large impact on the polariton scattering rates, giving rise to clear signatures in momentum-resolved absorption spectra that could be exploited to measure the energy of dark exciton states. Furthermore, we predict and explain a surprising difference in absorption intensity between the upper and lower polariton branch at zero momentum and zero detuning, despite equal photonic and excitonic contributions. We also study the influence of externally accessible quantities to tune the scattering rates (via temperature) and cavity decay rates (via mirror reflectance). For the latter, we find that the cavity quality factor plays an important role for the absorption, in particular for the lower polariton branch that has a smaller photonic component.

II. THEORY

We start by describing the theoretical approach to microscopically calculate the absorption spectrum for polaritons in TMD monolayers integrated into an optical cavity. Exciton energies and wavefunctions in TMD monolayers are obtained by solving the Wannier equation [14, 23, 24] including DFT input on single-particle energies [25]. TMDs are characterized by regular bright excitons that are directly accessible in optical spectra, as well as dark exciton states that are known to be the energetically lowest states in tungsten-based TMDs [13–16, 25, 26]. In this work, we focus on momentum-dark excitons consisting of Coulomb-bound electrons and holes that are located at different valleys within the Brillouin zone (K , K' or Λ). This means that the required large momentum transfer cannot be provided by photons, making these states optically

dark [12, 15, 26–29].

In this work, we combine the density matrix formalism with the Hopfield approach [10], to model the optical response of polaritons. We quantize separately a single internal cavity mode of a Fabry-Perot resonator and the external radiation fields, which are split into two sets of continuum modes corresponding to the left and the right of the cavity (Fig.1). The internal and external modes are weakly coupled via the end mirrors, where the in-plane wavevector is conserved. The starting point is the many-particle Hamiltonian in the excitonic picture $\hat{H} = \hat{H}_0 + \hat{H}_{X-c} + \hat{H}_{X-b} + \hat{H}_{B-c}$. The first term reads in second quantization

$$\begin{aligned} \hat{H}_0 = & \sum_{v\mathbf{k}} E_{v,\mathbf{k}}^X \hat{X}_{v\mathbf{k}}^\dagger \hat{X}_{v\mathbf{k}} + \sum_{\mathbf{k}} E_{\mathbf{k}}^c \hat{c}_{\mathbf{k}}^\dagger \hat{c}_{\mathbf{k}} + \sum_{\mathbf{q}} E_{\alpha\mathbf{q}}^b \hat{b}_{\alpha\mathbf{q}}^\dagger \hat{b}_{\alpha\mathbf{q}} \\ & + \sum_{j=L,R} \sum_{\mathbf{k}} \int_0^\infty d\omega \hbar\omega(\mathbf{k}) \hat{B}_{j\mathbf{k}\omega}^\dagger \hat{B}_{j\mathbf{k}\omega} \end{aligned} \quad (1)$$

and describes the free energy of excitons $E_{v\mathbf{k}}^X$, phonons $E_{\alpha\mathbf{q}}^b$ as well as photons within ($E_{\mathbf{k}}^c$) and outside the cavity ($\hbar\omega$). Here, v is the exciton index (we consider only 1s states), α the phonon mode, \mathbf{k} and \mathbf{q} are the in-plane momentum of excitons/photons (center-of-mass momentum for excitons) and phonons, respectively. Furthermore, we have introduced $\hat{X}_{v\mathbf{k}}^\dagger$ ($\hat{X}_{v\mathbf{k}}$), $\hat{b}_{\alpha\mathbf{q}}^\dagger$ ($\hat{b}_{\alpha\mathbf{q}}$), $\hat{c}_{\mathbf{k}}^\dagger$ ($\hat{c}_{\mathbf{k}}$), $\hat{B}_{j\mathbf{k}\omega}^\dagger$ ($\hat{B}_{j\mathbf{k}\omega}$) as exciton, phonon, inner-cavity and outer-cavity photon creation (and annihilation) operators, respectively.

The second term in the Hamiltonian, $\hat{H}_{X-c} = \sum_{v\mathbf{k}} g_{\mathbf{k}} (\hat{c}_{\mathbf{k}}^\dagger \hat{X}_{v\mathbf{k}} + \hat{c}_{\mathbf{k}} \hat{X}_{v\mathbf{k}}^\dagger)$ describes the exciton-light interaction mediated by the exciton-photon coupling matrix element $g_{\mathbf{k}}$ [14, 30], where photons need to have the same in-plane momentum \mathbf{k} as excitons to fulfill the momentum conservation (hence restricting the coupling only to the bright exciton states). In general, the out-of-plane component k_z influences the cavity energy and exciton-photon coupling. However, we assume the existence of one resonant photon mode (i.e., $E_{KK,0}^c = E_0^c$).

The third contribution in the Hamiltonian $\hat{H}_{X-b} = \sum_{vv'\mathbf{k}\alpha\mathbf{q}} \mathcal{D}_{\alpha\mathbf{q}}^{vv'} \hat{X}_{v\mathbf{k}+\mathbf{q}}^\dagger \hat{X}_{v'\mathbf{k}} (\hat{b}_{\alpha,-\mathbf{q}}^\dagger + \hat{b}_{\alpha\mathbf{q}})$ describes the exciton-phonon interaction [14], where the coupling strength is determined by the exciton-phonon matrix element $\mathcal{D}_{\alpha\mathbf{q}}^{vv'}$. Finally, the last term, $\hat{H}_{B-c} = i\hbar \sum_{j=L,R} \sum_{\mathbf{k}} \int_0^\infty \frac{d\omega}{2\pi} a_{j,\mathbf{k}}(\omega) [\hat{B}_{j\omega\mathbf{k}}^\dagger \hat{c}_{\mathbf{k}} - \hat{B}_{j\omega\mathbf{k}} \hat{c}_{\mathbf{k}}^\dagger]$, provides the interaction between the inner- and outer-cavity photons [19, 31]. The free photons interact with the cavity with a coupling parameter, $a_{j,\mathbf{k}}(\omega)$.

Assuming broadband end mirrors, it is appropriate to take the first Markov approximation and approximate this parameter as frequency independent [19]. This contribution in the Hamiltonian leads to a consistent description of both the radiative decay rate within the cavity as well as the coupling of polaritons to input and output fields.

Now, we investigate the strong-coupling regime, where the exciton-photon coupling strength $g_{\mathbf{k}}$ is larger than (the difference of) cavity and non-radiative exciton decay rates [11]. The new eigenmodes, known as exciton-polaritons, can be obtained by applying a Hopfield transformation of the excitonic Hamiltonian discussed above, yielding [10, 11]

$$\begin{aligned} \hat{H} = & \sum_{\mathbf{k},n} E_{\mathbf{k}}^n \hat{Y}_{\mathbf{k}}^{n\dagger} \hat{Y}_{\mathbf{k}}^n + H_b^0 + H_B^0 + \\ & + i\hbar \sum_{\mathbf{k},n,j} \int_0^\infty \frac{d\omega}{2\pi} a_{j\mathbf{k}}(\omega) \times \\ & \left(h_{C,\mathbf{k}}^n \hat{\mathcal{B}}_{j\mathbf{k}\omega}^\dagger \hat{Y}_{\mathbf{k}}^n - h_{C,\mathbf{k}}^{n*} \hat{\mathcal{B}}_{j\mathbf{k}\omega} \hat{Y}_{\mathbf{k}}^{n\dagger} \right) + \\ & + \sum_{\mathbf{k}\alpha\mathbf{q}n'n'} \tilde{D}_{\mathbf{k}\alpha\mathbf{q}}^{n'n} \left(\hat{b}_{\alpha,-\mathbf{q}}^\dagger + \hat{b}_{\alpha\mathbf{q}} \right) \hat{Y}_{\mathbf{k}+\mathbf{q}}^{n'\dagger} \hat{Y}_{\mathbf{k}}^n \quad (2) \end{aligned}$$

$$\begin{aligned} \hat{H} = & \sum_{\mathbf{k},n} E_{\mathbf{k}}^n \hat{Y}_{\mathbf{k}}^{n\dagger} \hat{Y}_{\mathbf{k}}^n + \sum_{\mathbf{k}\alpha\mathbf{q}n'n'} \tilde{D}_{\mathbf{k}\alpha\mathbf{q}}^{n'n} \left(\hat{b}_{\alpha,-\mathbf{q}}^\dagger + \hat{b}_{\alpha\mathbf{q}} \right) \hat{Y}_{\mathbf{k}+\mathbf{q}}^{n'\dagger} \hat{Y}_{\mathbf{k}}^n \\ & + i\hbar \sum_{\mathbf{k},n,j} \int_0^\infty \frac{d\omega}{2\pi} a_{j\mathbf{k}}(\omega) \left(h_{C,\mathbf{k}}^n \hat{\mathcal{B}}_{j\mathbf{k}\omega}^\dagger \hat{Y}_{\mathbf{k}}^n - h_{C,\mathbf{k}}^{n*} \hat{\mathcal{B}}_{j\mathbf{k}\omega} \hat{Y}_{\mathbf{k}}^{n\dagger} \right) \end{aligned}$$

Here, the first term provides the free polaritonic Hamiltonian with $\hat{Y}_{\mathbf{k}}^{n\dagger} (\hat{Y}_{\mathbf{k}}^n)$ denoting the polariton creation (annihilation) operator with the polariton mode n and momentum \mathbf{k} . The energy of the corresponding polariton, $E_{\mathbf{k}}^n$, includes in particular lower and upper polariton branches (LP, UP) that are separated in $k = 0$ by the Rabi splitting $\hbar\Omega_R = E_0^{UP} - E_0^{LP}$. This is a consequence of the mixing between excitons and photons (with the same center-of-mass and total momentum), as quantified by the Hopfield coefficients [11]. We include also, for notation convenience, polaritons steaming from momentum-dark excitons, although these show no exciton-photon mixing. Nevertheless, we will show below their crucial role for the polariton absorption via additional phonon-induced scattering channels to the optically active polaritons. Both polariton energies $E_{\mathbf{k}}^n$ and Hopfield coefficients $h_{X,\mathbf{k}}^n$ and $h_{c,\mathbf{k}}^n$ are calculated analytically (with subscript X and c referring to exciton and intra-cavity photon component, respectively) [11].

The second and the third term in Eq. (2) are the free phonon and free outer-cavity photon contribution, respectively, which are not affected by the Hopfield transformation. The fourth term describes the interaction of polaritons with the outer-cavity photons, mediated by the photonic Hopfield coefficients as only the photonic part of polaritons couples to the external radiation field. Finally, the last term in Eq. (2) describes the polariton-phonon interaction. Here, the matrix element \tilde{D} is related to the exciton-phonon coupling via $\tilde{D}_{\mathbf{k}\alpha\mathbf{q}}^{n'n} = h_{X,\mathbf{k}+\mathbf{q}}^{n'*} \mathcal{D}_{\alpha\mathbf{q}}^{n'n} h_{X,\mathbf{k}}^n$ and depends on the excitonic Hopfield coefficients h_X [32], since phonons only couple to the excitonic part of polaritons.

To obtain an expression for the polariton absorption, we exploit the Heisenberg equations of motion for the coherent population of polariton and external radiation field (cf. the supplementary information). For this we make a correlation expansion including the dynamics of the phonon-assisted polarization. We use the input-output method [19] to couple the dynamics between intra- and outer-cavity photon modes at each port. We treat the scattering with phonons within a Markov approximation and assuming a thermalized reservoir of incoherent phonons [15]. The absorption then follows from energy conservation as the difference between incoming fields and the total reflected and transmitted light. To simplify the resulting expression, we assume that the cavity is symmetric and ignore interference effects between polaritons in different branches. The latter is a good approximation if the branches are widely spaced in energy compared to the polaritonic spectral width. We obtain an Elliot-like formula for the polariton absorption [31],

$$A_{\mathbf{k}}^n(\hbar\omega) = \frac{4\gamma_{\mathbf{k}}^n \Gamma_{\mathbf{k}}^n}{(\hbar\omega - E_{\mathbf{k}}^n)^2 + (2\gamma_{\mathbf{k}}^n + \Gamma_{\mathbf{k}}^n)^2} \quad , \quad (3)$$

for each polariton branch and momentum n, \mathbf{k} . The obtained equation is similar to the expression found in Ref. [31], however, the key difference lies in the microscopic treatment of polariton-phonon interaction. This means that phonons can change the momentum of the excitonic component of the polariton, leading to a momentum dependent scattering rate. In Eq. (3) we introduced the decay rates

$$\gamma_{\mathbf{k}}^n = \hbar c(1 - |r_m|^2) |h_{c,\mathbf{k}}|^2 / (4L_{cav}) \quad (4)$$

$$\begin{aligned} \Gamma_{\mathbf{k}}^n = & 2\pi \sum_{n'\alpha\mathbf{k}'} |\tilde{D}_{\alpha,\mathbf{k}'-\mathbf{k}}^{n'n}|^2 \left(\frac{1}{2} \pm \frac{1}{2} + n_{\alpha,\mathbf{k}'-\mathbf{k}}^b \right) \times \\ & \times L_{\tilde{\gamma}_0} \left(E_{\mathbf{k}'}^{n'} - E_{\mathbf{k}}^n \pm E_{\alpha,\mathbf{k}'-\mathbf{k}}^b \right) \quad , \quad (5) \end{aligned}$$

where $\gamma_{\mathbf{k}}^n$ is the effective cavity decay rate of one port and $\Gamma_{\mathbf{k}}^n$ is the polariton-phonon scattering rate. Here we are summing over all possible scattering channels from a polariton n, \mathbf{k} to all possible receiving polaritons n', \mathbf{k}' via interaction with a phonon with mode α and momentum \mathbf{q} , such that the overall momentum is conserved. The quality factor of the cavity reads $Q_f = E_0^c L_{cav} / [\hbar c (1 - |r_m|^2)]$, where r_m is the reflectivity of the cavity. In this work, we use the default value of $r_m = 0.99$ if not stated otherwise. Importantly, we explicitly consider intervalley scattering by including K' and Q' phonons which allow scattering into polaritons coinciding with KK' and KA excitons, respectively. The polariton-phonon rates are calculated within the Markov-Born approximation [30, 33] including effects beyond the completed-collision limit [34] by an energy conservation described via a Lorentzian function with a broadening $\tilde{\gamma}_0 = 0.1$ meV [17].

Crucially, the polaritonic Elliot formula offers insight into how underlying microscopic decay channels manifest in the absorption of light by polaritons, which would not be possible using the more commonly used classical transfer-matrix method [18]. Evaluating Eq. (3) at resonance reveals that absorption is maximized when the two effective polariton decay rates are closest in value. It follows that maximum absorption of 0.5 is possible at the so-called critical coupling condition [22, 35] of $2\gamma_{\mathbf{k}}^n = \Gamma_{\mathbf{k}}^n$, i.e. when the leakage out of both ports of the cavity is equal to the exciton dissipation rate within the TMD layer in the cavity. The maximum possible absorption of 50% is a well-known constraint for mirror-symmetric two-port systems that support a single resonance [36, 37]. We expect the presence of dark excitons to significantly increase the polariton-phonon scattering rates in tungsten-based TMDs (as there they are the energetically lowest states). The opening of intervalley scattering channels is expected to strongly impact the balance between the effective radiative coupling and scattering loss, which should translate into measurable signatures in polariton absorption spectra.

III. RESULTS

A. Polariton absorption of WSe₂

Now, we evaluate Eq. (3), using numerically calculated polariton-phonon scattering rates, to study the polariton absorption in the strong-coupling regime for an hBN-encapsulated WSe₂ monolayer

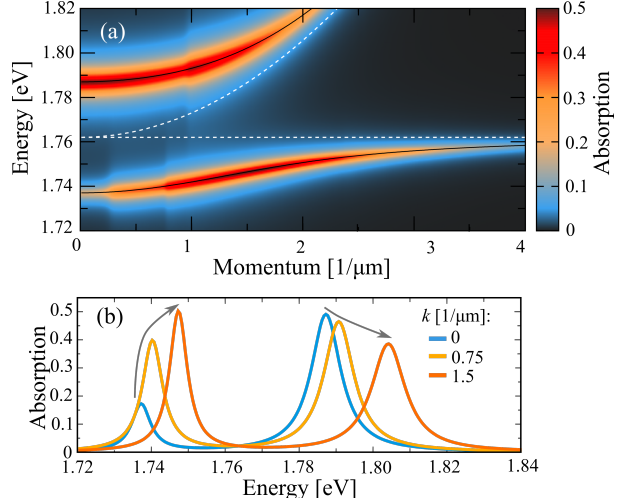


FIG. 2. Polariton absorption. (a) Surface plot of absorption in a hBN-encapsulated WSe₂ monolayer as a function of momentum and energy at a temperature of 77 K, assuming a Rabi splitting of $\hbar\Omega_R = 50$ meV and a cavity quality factor of $Q_f = 160$. The dashed white lines correspond to the bare exciton and cavity dispersion, while the solid black lines describe the polariton dispersion. (b) Absorption cuts as a function of energy for three different momenta.

integrated into a Fabry-Perot cavity with a quality factor of $Q_f \approx 160$ and a Rabi splitting of $\hbar\Omega_R = 50$ meV. Figure 2(a) presents an energy- and in-plane momentum-resolved surface plot of the polariton absorption. Interestingly, we find the upper polariton to be much higher in intensity than the lower polariton at $k = 0 \mu\text{m}^{-1}$ (cf. also the blue lines in Fig. 2(b)). Previous reports in GaAs have shown that in the case of zero detuning, the lower and upper polariton peaks intensities are similar [38, 39]. In the resonant case, the polaritons have an equal photonic and excitonic contribution at $k = 0$, hence also the cavity decay rate is the same for both polaritons. As a result, the phonon-induced decay rate of polaritons must be responsible for the observed difference in the height of absorption peaks. Furthermore, we find that the absorption is enhanced for increasing momenta for the lower polariton (A^{LP}) up to approximately $k = 1.6 \mu\text{m}^{-1}$, while it is reduced for the upper polariton (A^{UP}), (cf. also the absorption cuts in Fig. 2(b)). Moreover, we observe that not only the absorption intensity but also the linewidth of A^{LP} becomes larger for increasing in-plane momentum, before it is again reduced for momenta higher than $k = 1.6 \mu\text{m}^{-1}$. The absorption intensity and the spectral linewidth of polariton resonances can

be ascribed to the interplay of the cavity decay and non-radiative decay of polaritons via scattering with phonons as discussed in detail below.

B. Critical coupling

To explain the different behavior in the absorption spectra of the upper and lower polariton branch, we plot the maximal absorption $A_{\mathbf{k}}^n$ of the UP and the LP branch at 77 K in Fig. 3(a). The absorption intensity of the UP branch generally decreases with the momentum, however, with one exception at approximately $k = 1 \mu\text{m}^{-1}$, where we observe a small increase (blue line). For the lower polariton branch, then we find, in contrast, an enhanced absorption until approximately $k = 1.6 \mu\text{m}^{-1}$ where the critical coupling condition with a maximum possible value of $A = 0.5$, is reached (red line). The increase of the absorption includes several step-like enhancements before the absorption starts to decrease for values larger than $k = 1.6 \mu\text{m}^{-1}$.

To better understand the change of the absorption as a function of the in-plane momentum and the opposite behavior of the upper and the lower polariton branch observed in Fig. 3(a), we investigate the momentum-dependent cavity decay rate $\gamma_{\mathbf{k}}^n$ and polariton-phonon scattering rate $\Gamma_{\mathbf{k}}^n$, cf. Eqs. (4) and (5). We find that for the lower polariton branch, the critical coupling condition of $\Gamma_{\mathbf{k}}^n = 2\gamma_{\mathbf{k}}^n$ is reached at $k = 1.6 \mu\text{m}^{-1}$, as denoted with the black vertical line in Fig. 3(b). This corresponds exactly to the momentum where the maximal absorption of $A^{LP} = 0.5$ is reached. The microscopic calculation of polariton-photon scattering rates explains the step-like increase in the absorption of both the UP and LP polariton branch. These can be clearly attributed to an increase of the polariton-phonon scattering rates at certain momenta (at $k \approx 0.3, 0.8, 2.4$ and $3.1 \mu\text{m}^{-1}$ for $\Gamma_{\mathbf{k}}^{LP}$ and at $1 \mu\text{m}^{-1}$ for $\Gamma_{\mathbf{k}}^{UP}$). Importantly, each of these steep increases is a signature of an opening of an intervalley scattering channel into dark exciton states. At momentum $k = 0$, the energy E_0^{LP} of the lower polariton is too low to allow scattering into the $K\Lambda$ exciton via emission of phonons (Fig. 1(b)) as $E_0^{LP} - E_{\Lambda,0}^X \approx 11.2$ meV, which is just smaller than the energy of 11.4 meV of intervalley TA phonons [40]. When k reaches the threshold value of $k \approx 0.3 \mu\text{m}^{-1}$, the scattering channel into $K\Lambda$ states opens, resulting in the abrupt increase of $\Gamma_{\mathbf{k}}^n$, cf. also the schematic in Fig. 1(b). Note that, in contrast, the cavity decay rate $\gamma_{\mathbf{k}}^n$ increases/decreases smoothly with k for the UP/LP branch, cf. the dashed lines in Fig. 3(b). This in-

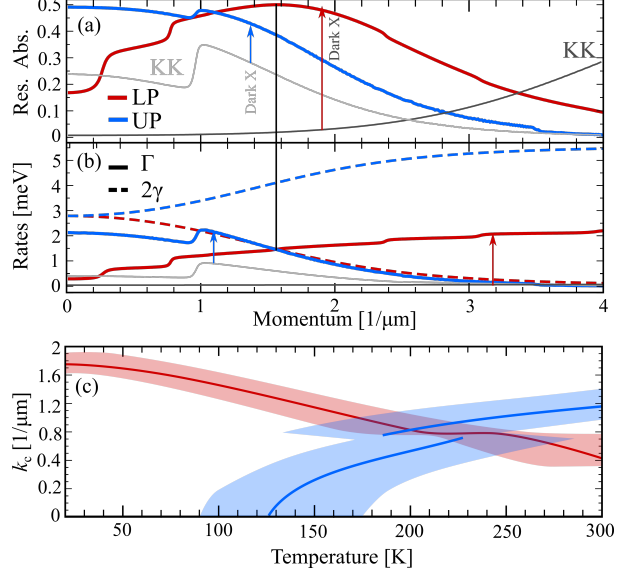


FIG. 3. Critical coupling. (a) Maximal absorption at the resonant energy as a function of momentum for the lower (red, LP) and upper (blue, UP) polariton at 77 K and $\hbar\Omega_R = 50$ meV, $Q_f \approx 160$. (b) Polariton-phonon scattering rate $\Gamma_{\mathbf{k}}^n$ (solid lines) and cavity decay rate $\gamma_{\mathbf{k}}^n$ (dashed lines) as a function of momentum for the upper and lower polariton (same colors as in (a)). The maximum value of absorption of $A^n = 0.5$ identifies the critical coupling conditions $\Gamma_{\mathbf{k}}^n = 2\gamma_{\mathbf{k}}^n$ for the respective polariton and it is marked by a vertical black line. The grey lines show the case without considering dark states and only taking into account the bright KK excitons. (c) Critical coupling momentum k_c as a function of temperature for the upper (blue) and lower polariton (red). The shaded area corresponds to the range $0.5 \geq A^n \geq 0.495$.

crease/decrease is determined by the photonic Hopfield coefficient, which increases for the UP and decreases for the LP branch.

To illustrate the importance of dark excitons, we also show the polariton absorption and the polariton-phonon scattering rates without including dark exciton states, i.e. we only take into account the bright KK excitons (grey lines in Figs. 3(a,b)). We find that for the lower polariton the resonant absorption is drastically reduced at small momenta, with the critical coupling condition shifted to higher momenta. We also find that the step increases step-like increases found for these polaritons disappear (red vs. lower grey line), as they stem from scattering into dark excitons. For the scattering rates of the lower polariton, the intravalley scattering is orders of magnitude smaller than the intervalley one (grey line is basically 0), due to the forbidden optical ab-

independent $2\gamma_0$, indicating at which temperatures the critical coupling condition is reached at $k_C = 0$. This is the case for the UP branch at $T \approx 125$ K - in agreement with Fig. 3(c). In contrast, for the LP branch, the critical coupling at $k_C = 0$ can only be reached at temperatures significantly higher than room temperature.

For both polariton branches, the largest contribution to the linewidth comes from the intervalley scattering into dark $K\Lambda$ excitons reflecting the efficient scattering plus the three-fold degeneracy of the Λ valley, similar to the excitonic case [41]. Furthermore, at room temperature, intervalley scattering within the K valley is also important. At 20K, the LP linewidth is determined to a large extent by scattering into the dark KK' excitons. We stress that here we are focusing on the scattering from the $k = 0$ polariton state. There are further possible scattering channels at larger momenta, as shown in Fig.3(b). Increasing the temperature to 300K increases the LP linewidth by around one order of magnitude as the absorption of intervalley phonons becomes possible. At 77 K the intravalley contribution to the phonon-scattering rates is very small, in accordance with Fig.3. The linewidth of the upper polariton is at 20K much larger compared to the LP branch since emission into dark excitons is possible even at $k = 0$ thanks to the much higher polariton energy (Fig. 1(b)). Hence, the increase in UP from 20K to 300K is not as substantial as in the LP case. Overall, Figs. 4(a,b) illustrate the huge impact of dark exciton states on the polariton-phonon scattering rates and thus on the polariton absorption.

After having addressed the role of temperature in tuning the polariton-phonon scattering rates $\Gamma_{\mathbf{k}}^n$, we now focus on the change of the cavity decay rate $\gamma_{\mathbf{k}}^n$ as a function of the quality factor Q_f . In Fig. 4(c) we show $\gamma_{\mathbf{k}}^n$ (gray line) and $\Gamma_{\mathbf{k}}^n$ (red and blue lines) as a function of Q_f . We find that UP has a critical coupling condition $k_C = 0$ around $Q_f \approx 200$. For small values of the quality factor, the UP absorption is expected to increase, but as we move further away from the critical coupling the absorption decreases. For the LP, the critical coupling condition is only reached at high values of Q_f .

D. Polariton absorption of MoSe₂

So far we have studied the polariton absorption for WSe₂ monolayers, where dark excitons turned out to play a crucial role. Now we investigate the MoSe₂ monolayer exhibiting a different energetic alignment of dark and bright states. With the latter being the

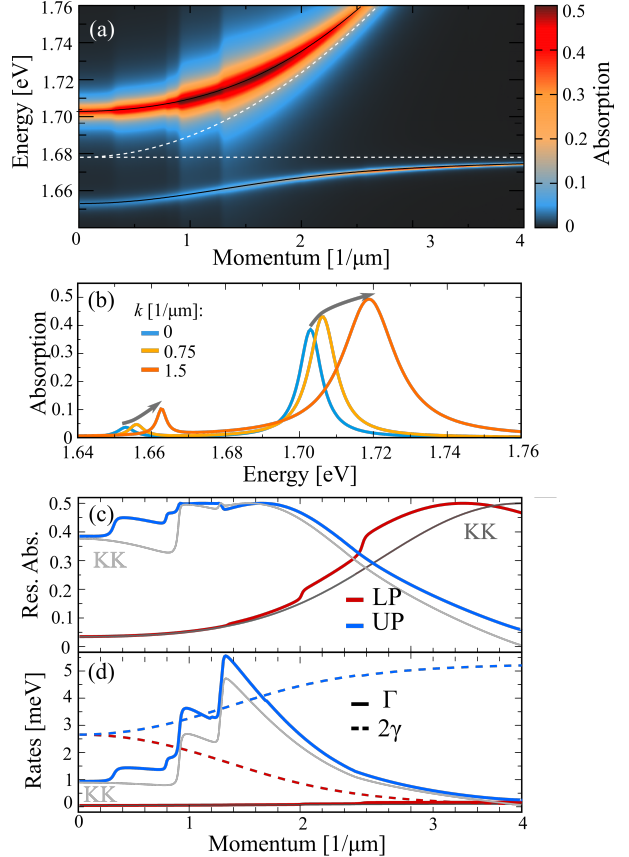


FIG. 5. Absorption of MoSe₂. (a) Surface plot of polariton absorption of a hBN-encapsulated MoSe₂ monolayer as a function of momentum and energy (77K, $\hbar\Omega_R = 50$ meV and $Q_f \approx 160$). (b) Absorption cuts as a function of energy for three different momenta. (c) Absorption intensity as a function of momentum for the lower (LP) and the upper (UP) polariton branch. (d) Decay rates $\Gamma_{\mathbf{k}}^n$ and $2\gamma_{\mathbf{k}}^n$ as a function of momentum for the LP and UP branch. The thin grey lines in (c) and (d) correspond to the case without dark excitons (considering only the bright KK excitons).

lowest ones in MoSe₂ [1, 14, 26], we expect only a negligible contribution from dark excitons. Similarly to the case of WSe₂, we show in Fig. 5(a) the absorption of polaritons as a function of momentum and energy for the zero-detuning case at $T = 77$ K. We find a drastic reduction in absorption as well as in the linewidth of the LP absorption compared to WSe₂ (Fig. 2(a)). This can be clearly observed in the momentum cuts shown in Fig. 5(b). Although the intensity of the resonant absorption increases for larger momenta, similar to the case of WSe₂, quantitatively the increase is much slower, reaching only a maximal value of approximately 0.1 at $k = 1.5\mu\text{m}^{-1}$

(compared to almost 0.5 predicted for WSe₂). Interestingly, for larger momenta we find also an increase of the absorption for the UP branch (Fig. 5(b)) - opposite to the case of WSe₂ (Fig. 2(b)). In addition, we observe a large increase in the spectral width of polariton resonances at larger in-plane momenta k .

To microscopically understand the qualitative as well as quantitative differences of the momentum-resolved absorption in MoSe₂ and WSe₂, we investigate the intensity of the resonant polariton absorption and the underlying polariton-phonon and cavity decay rates. We assume the same value of reflectivity $r_m = 0.99$ as in Fig. 2, resulting in similar cavity decay rates $\gamma_{\mathbf{k}}^n$ as for WSe₂. As a consequence, the observed difference in polariton absorption must be due to the phonon-scattering rates. We show both the absorption and decay rates also for the case without dark excitons (grey lines in Figs. 5(c,d)). As expected, in MoSe₂ there is only a minor contribution of dark states. For the LP branch, the scattering into the energetically higher dark exciton states is generally weak as it is driven by absorption of intervalley phonons from high-momenta states. Since for LP also the intravalley scattering with acoustic modes is forbidden due to momentum and energy conservation (due to the almost flat phonon dispersion making it difficult to fulfil the energy conservation [17]), the lower polariton has only a very small scattering rate (the red line in Fig. 4(d) is almost not visible). Nevertheless, the decrease of the cavity decay rate $\gamma_{\mathbf{k}}^n$ with increasing momenta allows for the critical coupling condition at the very high momenta of $k_c = 3.25 \mu\text{m}^{-1}$ (cf. Fig. 5(d)), where the LP absorption reaches its maximum value of $A^n = 0.5$ (Fig. 5(c)). Interestingly, even though dark excitons have only a small contribution, their presence shifts the critical coupling condition to a smaller momentum (cf. grey vs red line in Fig. 5(c)).

For the upper polariton, the intra-valley scattering contribution is also dominant (only small deviations between the grey and blue line), showing two step-like increases at $k \approx 1$ and $k \approx 1.3 \mu\text{m}^{-1}$ due to the emission of intravalley optical modes (LO/TO and A1 with energy 36.1/36.6 meV and 30.3 meV, respectively). In contrast to WSe₂, we observe a large increase in the phonon-scattering rates for the UP branch, reflecting a more efficient intravalley scattering with optical modes in MoSe₂ [40]. This leads to the much broader spectral width of the resonances observed in Fig. 5(b). The contribution of dark excitons is minor, however, we still observe an opening of an emission channel into dark states, cf. the step-like increase of $\Gamma_{\mathbf{k}}^{UP}$ at $k \approx 0.4 \mu\text{m}^{-1}$. This opening is important for understanding the increase

of the resonant absorption, when going from $k = 0$ to $k = 0.75 \mu\text{m}^{-1}$ observed in Fig. 5(b) (in contrast to the prediction for WSe₂ in Fig. 1(a)). Without dark states, there would be a decrease of the absorption up to approximately $0.9 \mu\text{m}^{-1}$ (cf. the grey line in Fig. 5(c)). In MoSe₂, the upper polariton fulfills the critical coupling condition at the four different momenta $k_c \approx 1, 1.2, 1.3$ and $1.6 1/\mu\text{m}$. The lowest two are a consequence of polariton scattering into dark exciton states.

IV. CONCLUSION

We have studied polariton absorption for hBN-encapsulated WSe₂ and MoSe₂ monolayers integrated into a Fabry-Perot cavity. These two materials are ideal to study the impact of momentum-dark exciton states, as they possess an opposite energetic ordering of bright and dark states. Based on a microscopic theory combining the Hopfield approach with an excitonic density matrix formalism, we predict a significant impact of dark excitons on the polariton absorption in WSe₂. This is particularly true for the absorption of the lower-polariton branch, which shows an overall enhancement of the absorption intensity as well as a distinctive step-like increase in momentum-resolved resonant absorption. The latter indicate the opening of scattering channels into dark exciton states, hence potentially suggesting a possibility to measure the energy of dark excitons. Furthermore, we have investigated the critical coupling condition at which a maximum possible absorption intensity can be reached. To tune this condition, we have varied temperature and the cavity quality factor allowing us to control the polariton-phonon scattering rates and cavity decay rates, respectively. Our study provides new microscopic insights into the polariton absorption and the role of dark exciton states and could trigger further experimental studies on exciton-polaritons in atomically-thin materials.

ACKNOWLEDGMENTS

We thank Marten Richter (TU Berlin) for inspiring discussions. This project has received funding support from the DFG via SFB 1083 (project B9), the European Union's Horizon 2020 Research and Innovation programme under grant agreement no. 881603 (Graphene Flagship) and from the Knut and Alice Wallenberg Foundation via the Grant KAW 2019.0140. The computations were enabled

-
- [1] T. Mueller and E. Malic, Exciton physics and device application of two-dimensional transition metal dichalcogenide semiconductors, *npj 2D Mater. Appl.* **2**, 29 (2018).
- [2] G. Berghäuser, P. Steinleitner, P. Merkl, R. Huber, A. Knorr, and E. Malic, Mapping of the dark exciton landscape in transition metal dichalcogenides, *Phys. Rev. B* **98**, 020301 (2018).
- [3] K. He, N. Kumar, L. Zhao, Z. Wang, K. F. Mak, H. Zhao, and J. Shan, Tightly bound excitons in monolayer WSe₂, *Phys. Rev. Lett.* **113**, 026803 (2014).
- [4] M. M. Ugeda, A. J. Bradley, S.-F. Shi, H. Felipe, Y. Zhang, D. Y. Qiu, W. Ruan, S.-K. Mo, Z. Hussain, Z.-X. Shen, F. Wang, S. G. Louie, and M. F. Crommie, Giant bandgap renormalization and excitonic effects in a monolayer transition metal dichalcogenide semiconductor, *Nat. Mat.* **13**, 1091 (2014).
- [5] G. Wang, A. Chernikov, M. M. Glazov, T. F. Heinz, X. Marie, T. Amand, and B. Urbaszek, Colloquium: Excitons in atomically thin transition metal dichalcogenides, *Rev. Mod. Phys.* **90**, 1 (2018).
- [6] M. N. Brunetti, O. L. Berman, and R. Y. Kezrashvili, Optical absorption by indirect excitons in a transition metal dichalcogenide/hexagonal boron nitride heterostructure, *J. Phys. Condens. Matter* **30**, 225001 (2018).
- [7] X. Liu, T. Galfsky, Z. Sun, F. Xia, E.-c. Lin, Y.-H. Lee, S. Kéna-Cohen, and V. M. Menon, Strong light-matter coupling in two-dimensional atomic crystals, *Nat. Photon.* **9**, 30 (2015).
- [8] S. Dufferwiel, S. Schwarz, F. Withers, A. Trichet, F. Li, M. Sich, O. Del Pozo-Zamudio, C. Clark, A. Nalitov, D. Solnyshkov, *et al.*, Exciton-polaritons in Van der Waals heterostructures embedded in tunable microcavities, *Nat. Commun.* **6**, 1 (2015).
- [9] C. Schneider, M. M. Glazov, T. Korn, S. Höfling, and B. Urbaszek, Two-dimensional semiconductors in the regime of strong light-matter coupling, *Nat. Commun.* **9**, 1 (2018).
- [10] J. Hopfield, Theory of the contribution of excitons to the complex dielectric constant of crystals, *Phys. Rev.* **112**, 1555 (1958).
- [11] H. Deng, H. Haug, and Y. Yamamoto, Exciton-polariton Bose-Einstein condensation, *Rev. Mod. Phys.* **82**, 1489 (2010).
- [12] E. Malic, M. Selig, M. Feierabend, S. Brem, D. Christiansen, F. Wendler, A. Knorr, and G. Berghäuser, Dark excitons in transition metal dichalcogenides, *Phys. Rev. Mater.* **2**, 014002 (2018).
- [13] X.-X. Zhang, Y. You, S. Y. F. Zhao, and T. F. Heinz, Experimental evidence for dark excitons in monolayer WSe₂, *Phys. Rev. Lett.* **115**, 257403 (2015).
- [14] M. Selig, G. Berghäuser, A. Raja, P. Nagler, C. Schüller, T. F. Heinz, T. Korn, A. Chernikov, E. Malic, and A. Knorr, Excitonic linewidth and coherence lifetime in monolayer transition metal dichalcogenides, *Nat. Commun.* **7**, 13279 (2016).
- [15] S. Brem, A. Ekman, D. Christiansen, F. Katsch, M. Selig, C. Robert, X. Marie, B. Urbaszek, A. Knorr, and E. Malic, Phonon-assisted photoluminescence from indirect excitons in monolayers of transition-metal dichalcogenides, *Nano Lett.* **20**, 2849 (2020).
- [16] R. Rosati, R. Schmidt, S. Brem, R. Perea-Causín, I. Niehues, J. Kern, J. A. Preuß, R. Schneider, S. Michaelis de Vasconcellos, R. Bratschitsch, and E. Malic, Dark exciton anti-funneling in atomically thin semiconductors, *Nature Commun.* **12**, 7221 (2021).
- [17] B. Ferreira, R. Rosati, and E. Malic, Microscopic modeling of exciton-polariton diffusion coefficients in atomically thin semiconductors, *Phys. Rev. Mat.* **6**, 034008 (2022).
- [18] A. V. Kavokin, J. J. Baumberg, G. Malpuech, and F. P. Laussy, *Microcavities*, Vol. 21 (Oxford university press, 2017).
- [19] C. W. Gardiner and M. J. Collett, Input and output in damped quantum systems: Quantum stochastic differential equations and the master equation, *Phys. Rev. A* **31**, 3761 (1985).
- [20] M. Selig, G. Berghäuser, M. Richter, R. Bratschitsch, A. Knorr, and E. Malic, Dark and bright exciton formation, thermalization, and photoluminescence in monolayer transition metal dichalcogenides, *2D Materials* **5**, 035017 (2018).
- [21] S. Brem, C. Linderlav, P. Erhart, and E. Malic, Tunable phases of moiré excitons in van der waals heterostructures, *Nano letters* **20**, 8534 (2020).
- [22] H. Haus, *Waves and fields in optoelectronics.*, PRENTICE-HALL, INC., ENGLEWOOD CLIFFS, NJ 07632, USA, 1984, 402 (1984).
- [23] H. Haug and S. W. Koch, *Quantum Theory of the Optical and Electronic Properties of Semiconductors: Fifth Edition* (World Scientific Publishing Company, 2009).
- [24] G. Berghäuser and E. Malic, Analytical approach to excitonic properties of MoS₂, *Phys. Rev. B* **89**, 125309 (2014).

- [25] A. Kormányos, G. Burkard, M. Gmitra, J. Fabian, V. Zólyomi, N. D. Drummond, and V. Fal'ko, k-p theory for two-dimensional transition metal dichalcogenide semiconductors, *2D Mater.* **2**, 022001 (2015).
- [26] T. Deilmann and K. S. Thygesen, Finite-momentum exciton landscape in mono- and bilayer transition metal dichalcogenides, *2D Mater.* **6**, 035003 (2019).
- [27] M. Feierabend, G. Berghäuser, A. Knorr, and E. Malic, Proposal for dark exciton based chemical sensors, *Nat. Commun.* **8**, 1 (2017).
- [28] D. Erkensten, S. Brem, K. Wagner, R. Gillen, R. Perea-Causín, J. D. Ziegler, T. Taniguchi, K. Watanabe, J. Maultzsch, A. Chernikov, and E. Malic, Dark exciton-exciton annihilation in monolayer WSe₂, *Phys. Rev. B* **104**, L241406 (2021).
- [29] R. Wallauer, R. Perea-Causin, L. Munster, S. Zajączek, S. Brem, J. Gudde, K. Tanimura, K.-Q. Lin, R. Huber, E. Malic, *et al.*, Momentum-resolved observation of exciton formation dynamics in monolayer WS₂, *Nano Lett.* **21**, 5867 (2021).
- [30] S. Brem, M. Selig, G. Berghäuser, and E. Malic, Exciton relaxation cascade in two-dimensional transition metal dichalcogenides, *Sci. Rep.* **8**, 8238 (2018).
- [31] J. M. Fitzgerald, J. J. Thompson, and E. Malic, Twist angle tuning of moiré exciton polaritons in van der waals heterostructures, *Nano Lett.* **22**, 4468 (2022).
- [32] F. Lengers, T. Kuhn, and D. E. Reiter, Phonon signatures in spectra of exciton polaritons in transition metal dichalcogenides, *Phys. Rev. B* **104**, L241301 (2021).
- [33] A. Thränhardt, S. Kuckenburg, A. Knorr, T. Meier, and S. Koch, Quantum theory of phonon-assisted exciton formation and luminescence in semiconductor quantum wells, *Phys. Rev. B* **62**, 2706 (2000).
- [34] F. Rossi, *Theory of semiconductor quantum devices: microscopic modeling and simulation strategies* (Springer Science & Business Media, 2011).
- [35] R. B. Adler, L. J. Chu, and R. M. Fano, *Electromagnetic energy transmission and radiation* (Wiley, 1960).
- [36] L. Botten, R. McPhedran, N. Nicorovici, and G. Derrick, Periodic models for thin optimal absorbers of electromagnetic radiation, *Phys. Rev. B* **55**, R16072 (1997).
- [37] J. R. Piper, V. Liu, and S. Fan, Total absorption by degenerate critical coupling, *Appl. Phys. Lett.* **104**, 251110 (2014).
- [38] Y. Chen, A. Tredicucci, and F. Bassani, Bulk exciton polaritons in GaAs microcavities, *Phys. Rev. B* **52**, 1800 (1995).
- [39] S. Pau, G. Björk, J. Jacobson, H. Cao, and Y. Yamamoto, Microcavity exciton-polariton splitting in the linear regime, *Phys. Rev. B* **51**, 14437 (1995).
- [40] Z. Jin, X. Li, J. T. Mullen, and K. W. Kim, Intrinsic transport properties of electrons and holes in monolayer transition-metal dichalcogenides, *Phys. Rev. B* **90**, 045422 (2014).
- [41] S. Brem, J. Zipfel, M. Selig, A. Raja, L. Waldecker, J. D. Ziegler, T. Taniguchi, K. Watanabe, A. Chernikov, and E. Malic, Intrinsic lifetime of higher excitonic states in tungsten diselenide monolayers, *Nanoscale* **11**, 12381 (2019).